SUPPLEMENTARY FIGURES - Kv4.3 channel downregulation mediates chronic post-lesional pacemaker acceleration in surviving dopamine substantia nigra neurons

Lora Kovacheva[1], Josef Shin, Navid Farassat[*] & Jochen Roeper[1]

Institute of Neurophysiology, Neuroscience Center, Goethe University, Frankfurt, Germany.

*Present address: Eye Center, Medical Center, Medical Faculty, Albert-Ludwig University Freiburg, Germany

[1] Corresponding authors:

Prof. Dr. Jochen Roeper & Lora Kovacheva

Institute for Neurophysiology

Neuroscience Center, Goethe University

Theodor-Stern-Kai 7, 60590 Frankfurt, Germany

e-mail: roeper@em.uni-frankfurt.de & email: lorask@gmail.com

Tel: +49-69-6301-84091/92

Supplementary Figure 1.

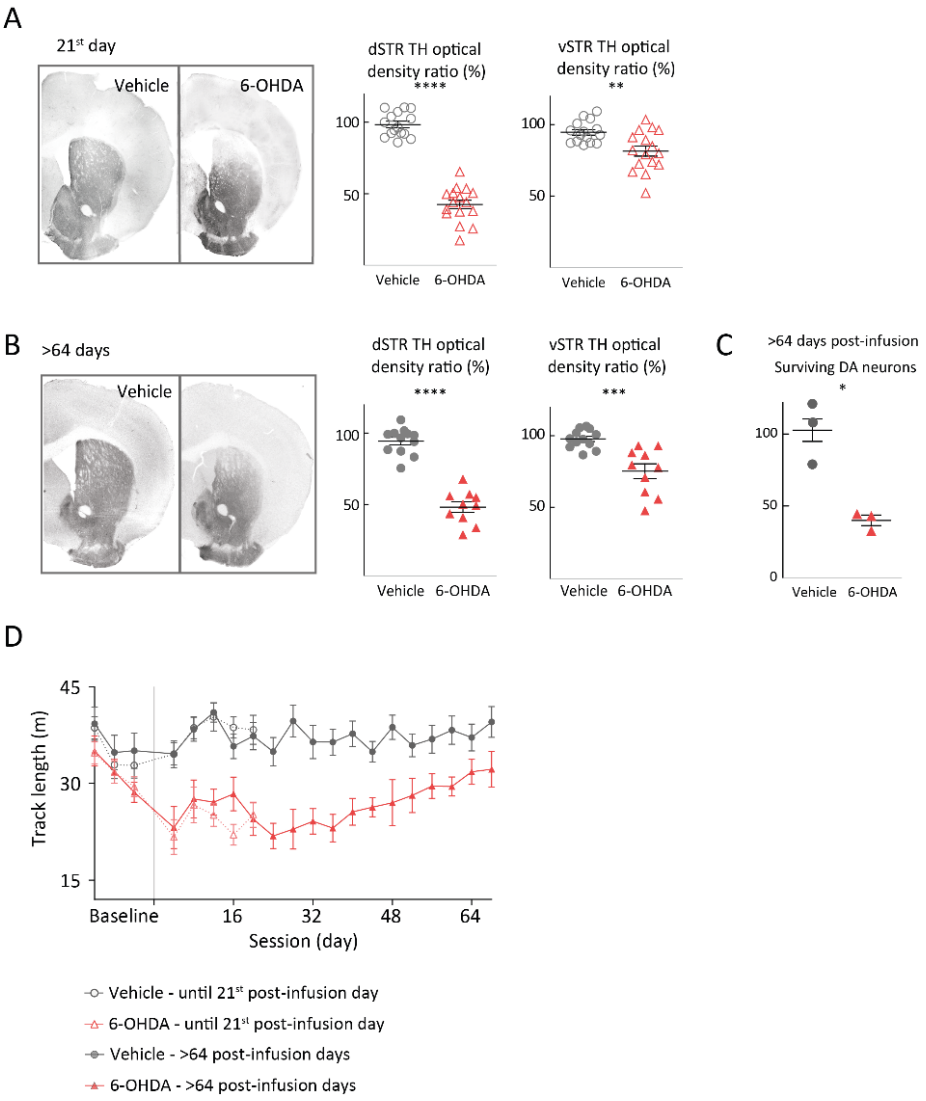

(A), (B) Comparison of ipsilateral, infusion side, to contralateral side as percentage of relative TH immunohistochemistry signal in the dorsal striatum (dSTR) and ventral striatum (vSTR), at the corresponding early (A) and late phase (B). Note the stability of TH density loss in the dorsal striatum through time. (C) Ratio of ipsilateral (infusion side) to contralateral side of surviving TH-positive neurons in SN in the late phase. (D) Mean track length from all mice for each open field session. Note the post-infusion drop in performed track in the 6-OHDA groups, which gradually recovers. (Infusion day marked as a thin gray line.)

Supplementary Figure 2.

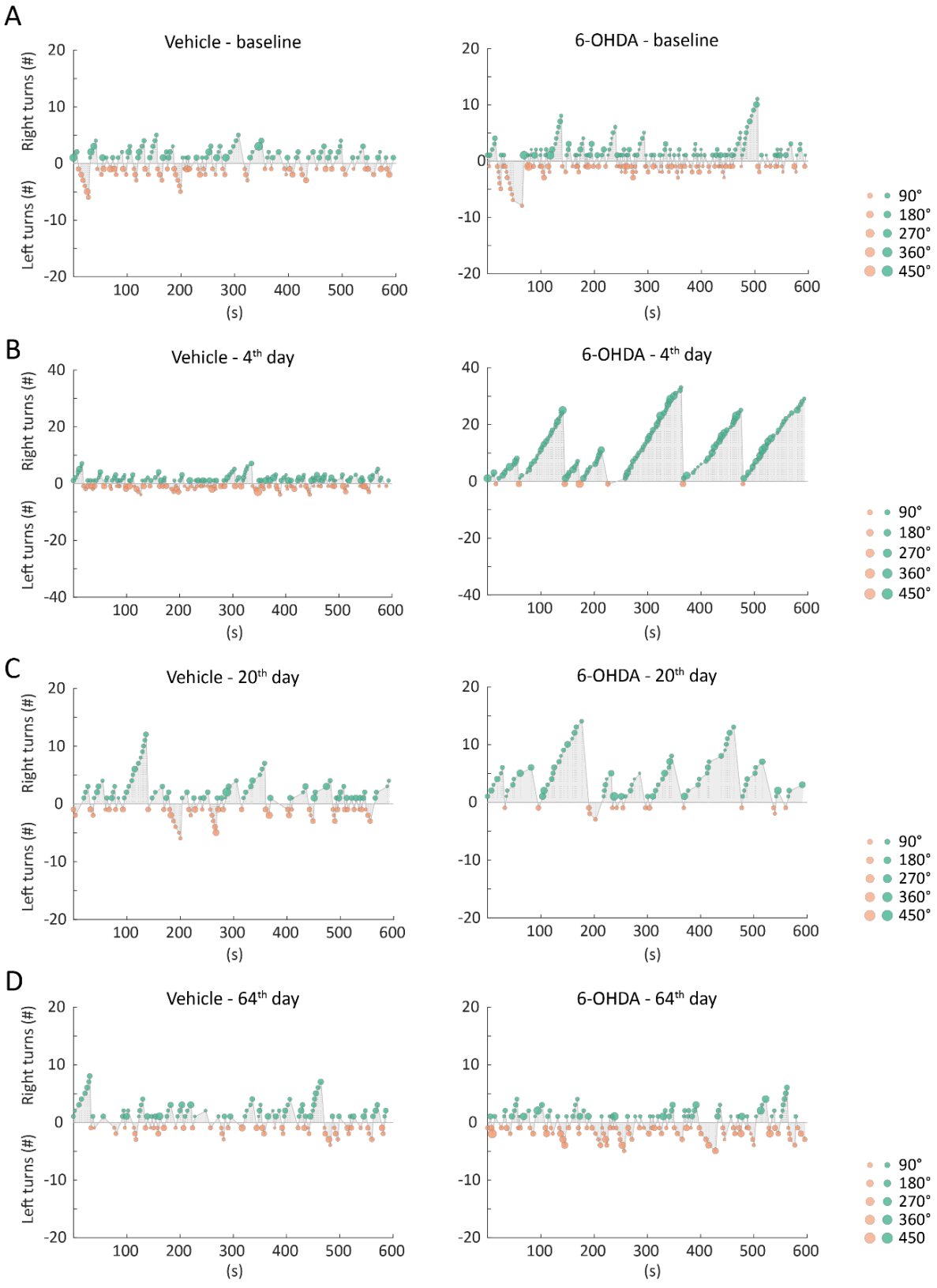

For two representative vehicle- and 6-OHDA-treated mice schematic representation of turning sequences. Left turn sequences are plotted as negative values, whereas right turn sequences are plotted as positive values. The count represents the number of same-direction turns within a

sequence. On the left panels are turning sequences for the control animal and on the right panels for the 6-OHDA-infused animal, correspondingly in a baseline session (A), 4th post-operative day (B), 20th post-operative day (C) and 64th post-operative day (D).

Supplementary Figure 3.

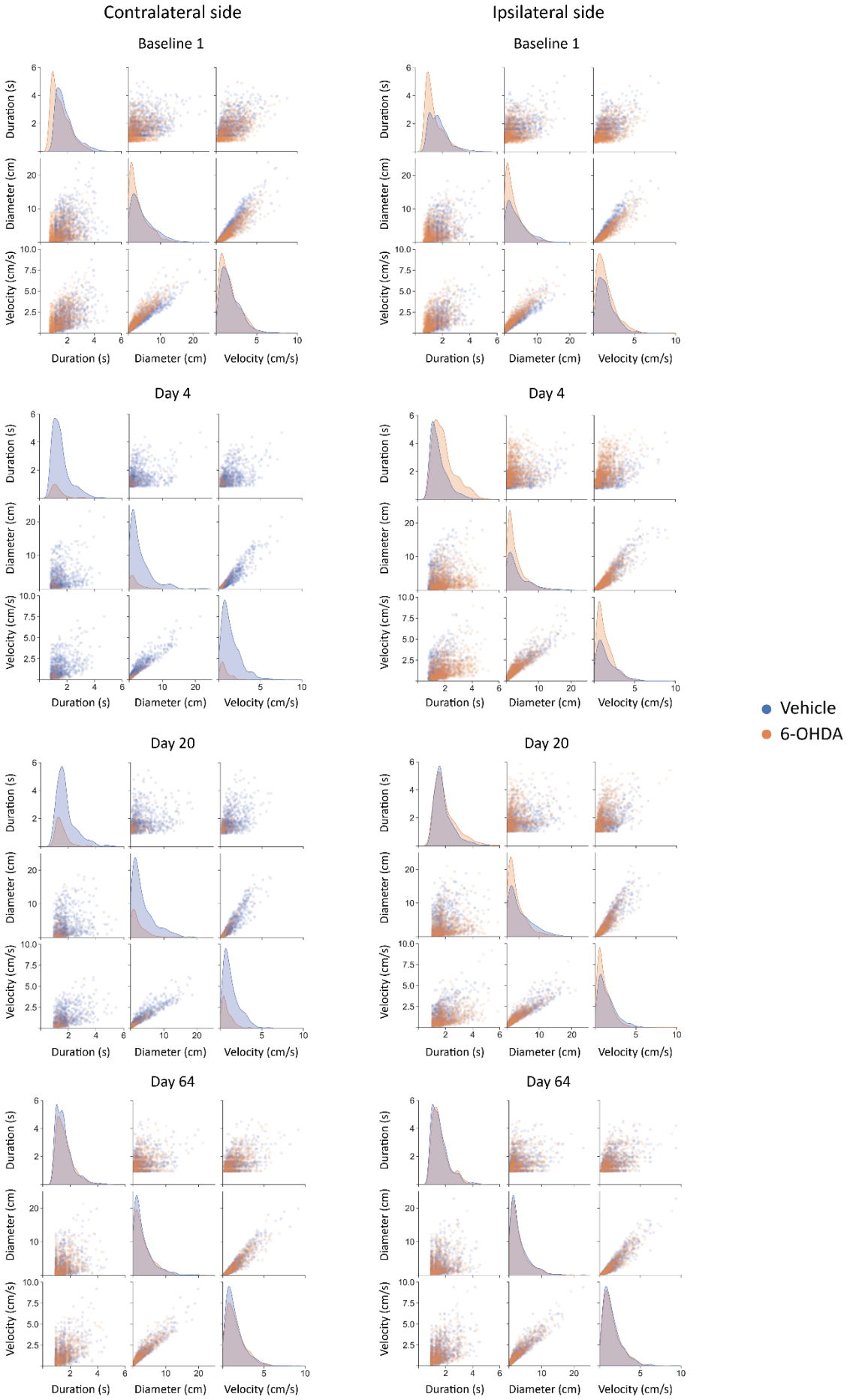

Correlation pair plots comparing turning features, such as velocity (cm/s), diameter (cm) and duration for all contralateral turns (left panels) and all ipsilateral turns performed from all vehicle-infused mice (in orange) and all 6-OHDA-treated mice (in blue) across different time points (baseline, 4^{th}, 20^{th} and 64^{th} post-infusion day).

Supplementary Figure 4.

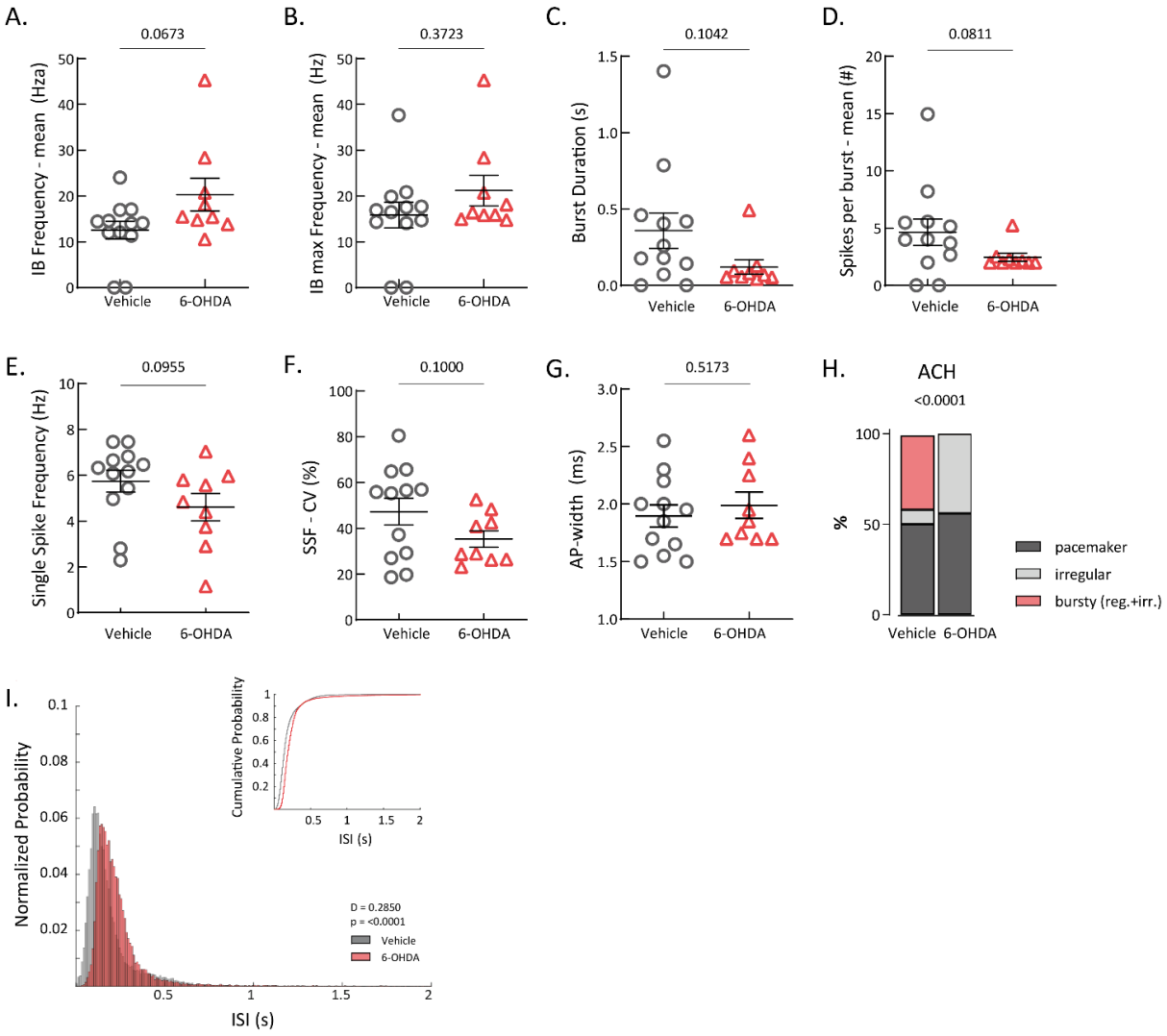

Scatter dot-plots, showing no significant difference of *in vivo* mean intra-burst (IB) frequency (A), mean maximum (max) intra-burst (IB) frequency (B), burst duration (C), number of spikes per burst (D), single spike frequency (SSF) (E), single spike coefficient of variance (CV) (F) and action potential (AP) width (G) (H) between the vehicle and 6-OHDA-infused mice in the early phase. (H) Normalized stacked bar plots of different *in vivo* firing patterns based on ACH. (I) ISI distributions from all *in vivo* recorded and labeled mSN DA neurons from vehicle- and 6-OHDA-treated mice in the early phase. Inset, cumulative representation of the same distributions.

Supplementary Figure 5.

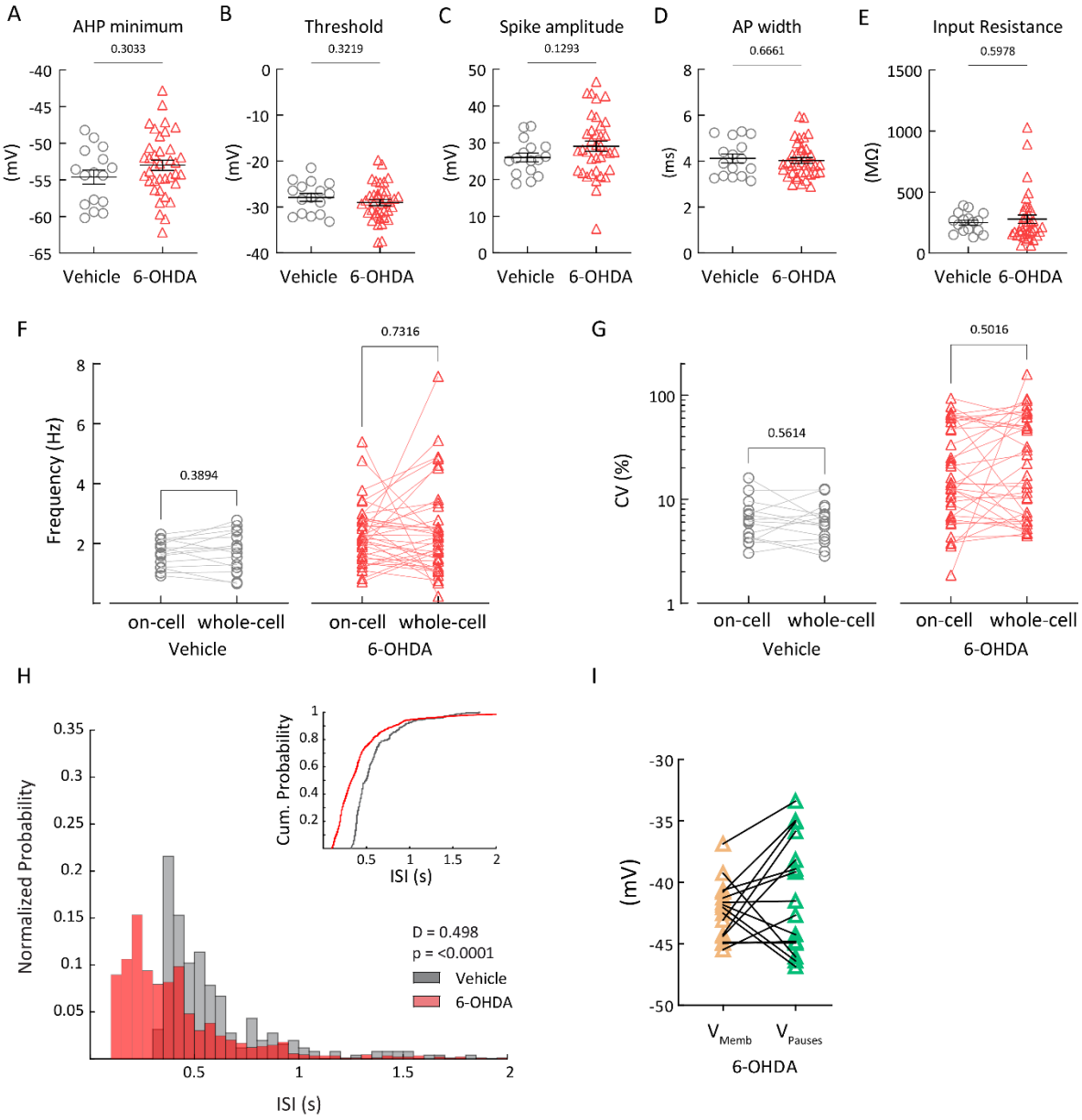

Scatter dot-plots, showing no significant difference of *in vitro* afterhyperpolarization (AHP) minimum (A), threshold (B), spike amplitude (C), action potential (AP) width (D) and input resistance (E) between the vehicle and 6-OHDA-infused mice in the early phase. (F), (G) Paired scatter dot-plots of firing frequency (F) and coefficient of variance (G) during on-cell recording and whole-cell recording in the early phase. (H) ISI distributions from all *in vitro* whole-cell recorded and labeled mSN DA neurons from vehicle- and 6-OHDA-treated mice in the early phase. Inset, cumulative representation of the same distributions. (I) Paired scatter dot-plot indicating no significant difference between the mean voltage during spike-pauses and the rest of the firing activity.

Supplementary Figure 6.

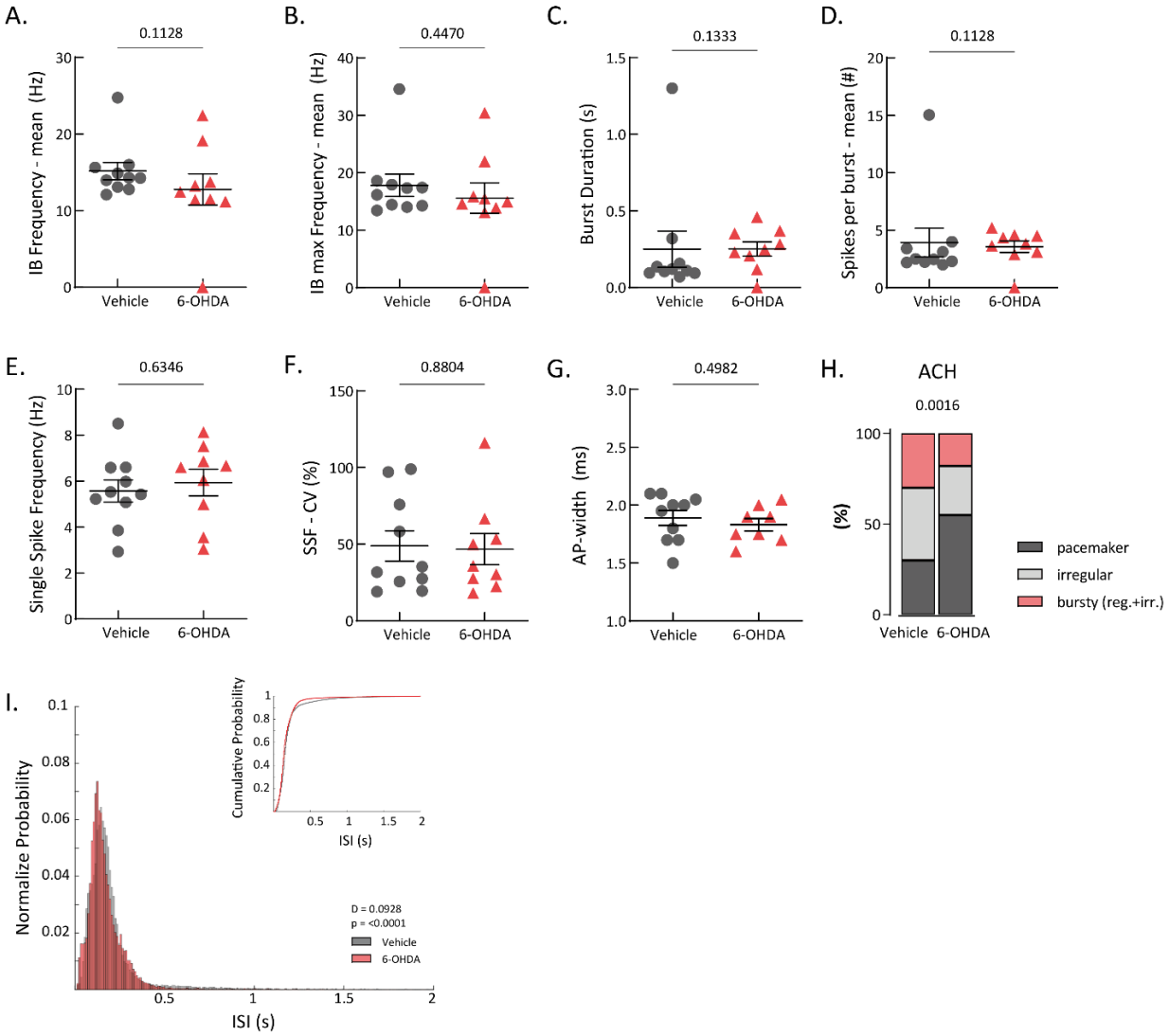

Scatter dot-plots, showing no significant difference of *in vivo* mean intra-burst (IB) frequency (A), mean maximum (max) intra-burst (IB) frequency (B), burst duration (C), number of spikes per burst (D), single spike frequency (SSF) (E), single spike coefficient of variance (CV) (F) and action potential (AP) width (G) (H) between the vehicle and 6-OHDA-infused mice in the late phase. (H) Normalized stacked bar plots of different *in vivo* firing patterns based on ACH. (I) ISI distributions from all *in vivo* recorded and labeled mSN DA neurons from vehicle- and 6-OHDA-treated mice in the late phase. Inset, cumulative representation of the same distributions.

Supplementary Figure 7.

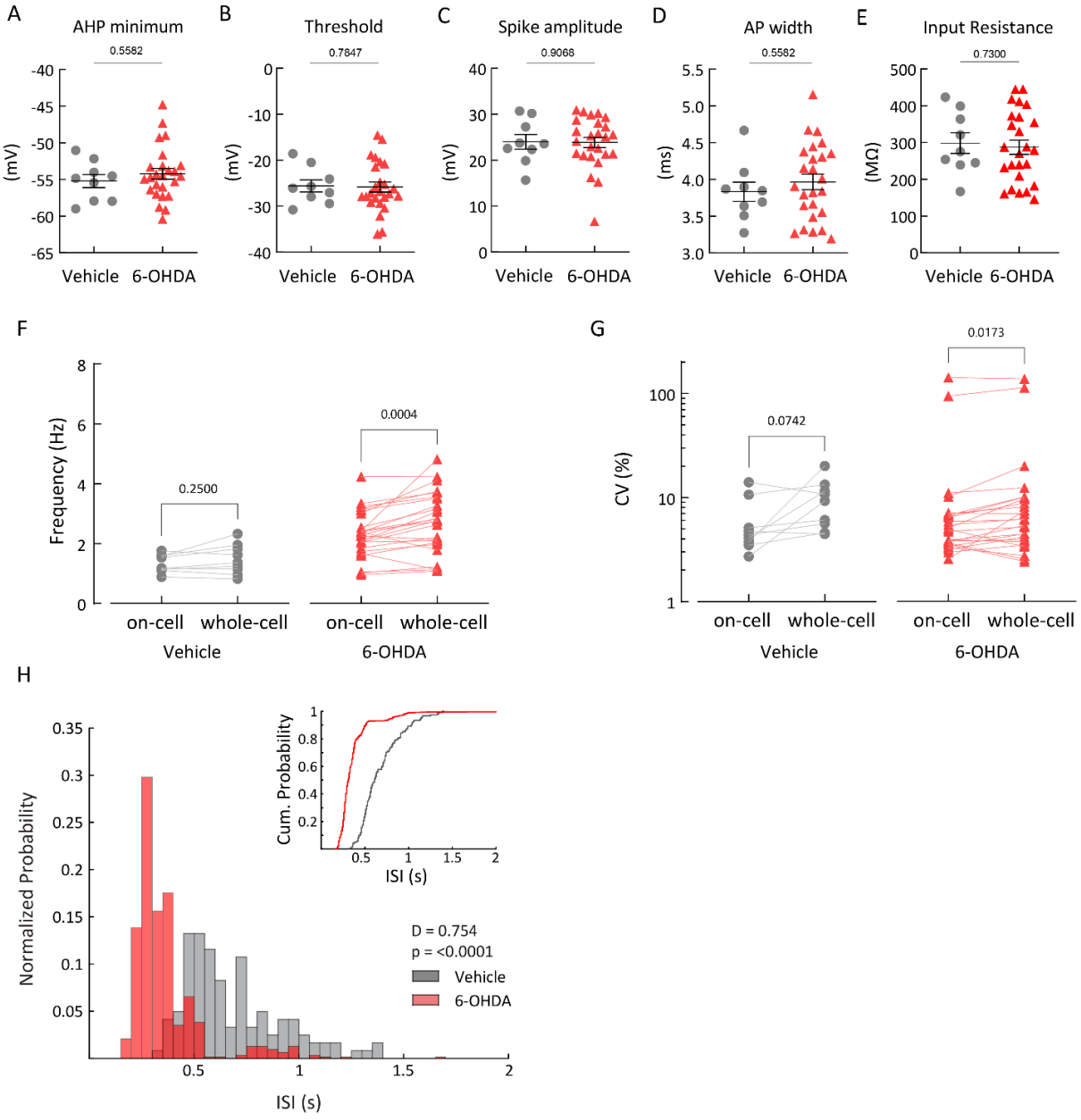

Scatter dot-plots, showing no significant difference of *in vitro* afterhyperpolarization (AHP) minimum (A), threshold (B), spike amplitude (C), action potential (AP) width (D) and input resistance (E) between the vehicle and 6-OHDA-infused mice in the late phase. (F), (G) Paired scatter dot-plots of firing frequency (F) and coefficient of variance (G) during on-cell recording and whole-cell recording in the late phase. (H) ISI distributions from all *in vitro* whole-cell recorded and labeled mSN DA neurons from vehicle- and 6-OHDA-treated mice in the late phase. Inset, cumulative representation of the same distributions.

Supplementary Figure 8.

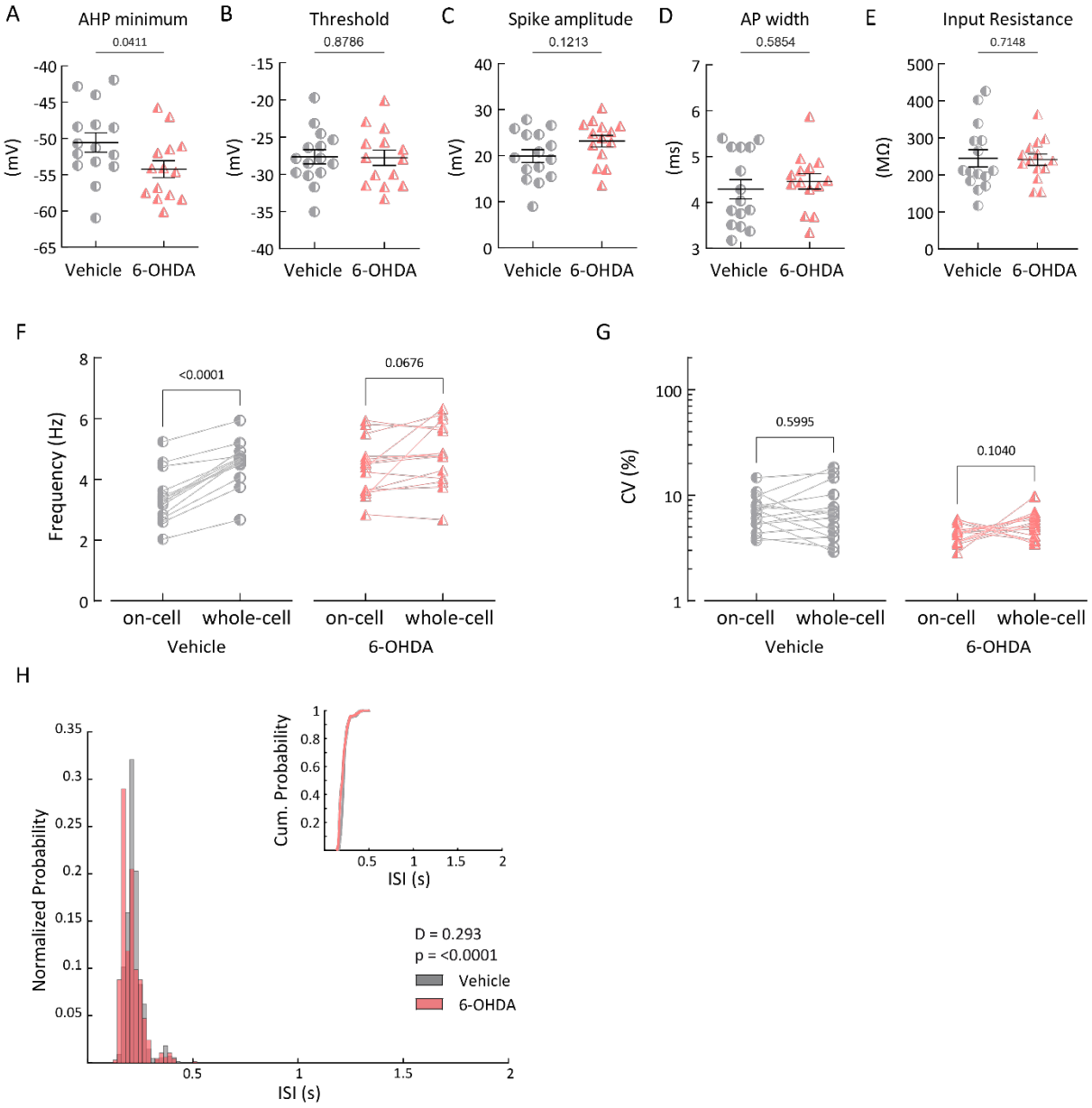

Scatter dot-plots, showing minor significant difference of *in vitro* afterhyperpolarization (AHP) minimum (A), and no difference in threshold (B), spike amplitude (C), action potential (AP) width (D) and input resistance (E) between the vehicle and 6-OHDA-infused mice in the late phase under 1µM AmmTx3. (F), (G) Paired scatter dot-plots of firing frequency (F) and coefficient of variance (G) during on-cell recording and whole-cell recording in the late phase under 1µM AmmTx3. (H) ISI distributions from all *in vitro* whole-cell recorded and labeled mSN DA neurons from vehicle- and 6-OHDA-treated mice in the late phase under 1µM AmmTx3. Inset, cumulative representation of the same distributions.

Supplementary Figure 9.

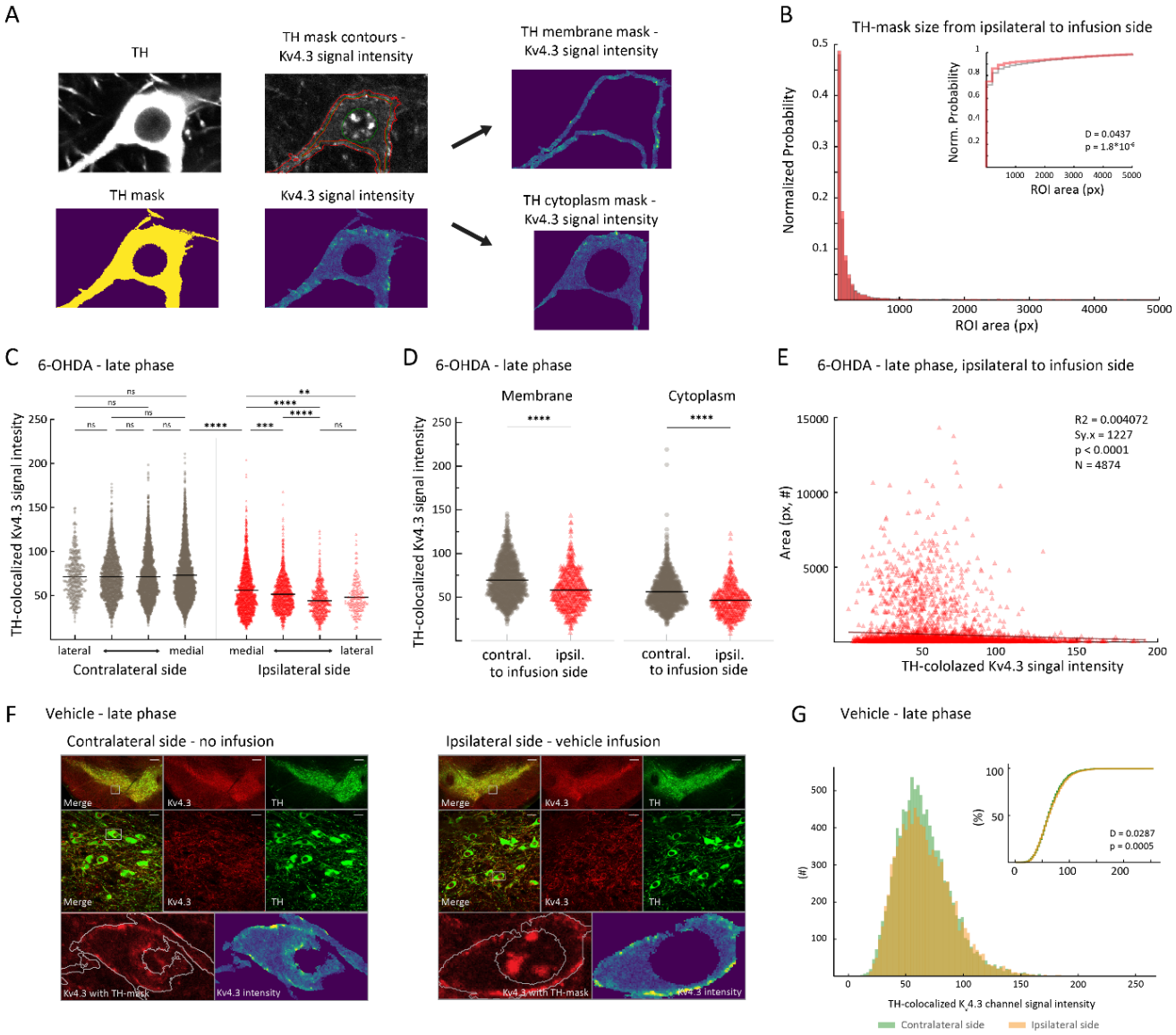

(A) Example illustration of an image from neuronal TH-immunosignal, transformed as a TH mask and overlayed on top of Kv4.3 immunosignal. Further segregation of the membrane and cytoplasm compartment with the corresponding Kv4.3 immunosignal intensity. (B) Distributions of all ROIs area sizes based on TH-masks from vehicle- (gray) and 6-OHDA-treated mice (red) in the late phase. Inset, cumulative representation of the same distributions. (C) Scatter dot-plots, illustrating the medio-lateral gradient of Kv4.3 immunosignal on the contralateral and ipsilateral side from 6-OHDA-treated mice in the late phase. (D) Scatter dot-plots, showing significant decrease in Kv4.3 immunosignal in both membrane and cytoplasm compartments in the ipsilateral (6-OHDA-infused) side compared to the contralateral (control) side. (E) Correlation of Kv4.3 immunosignal to ROI area size showed, based

on all ROIs from ipsilateral to infusion side from 6-OHDA-treated mice in the late phase. (F) Top: 4x magnification of midbrain of a vehicle-infused mouse, >64 days post-lesion – contralateral side (left panel), and corresponding ipsilateral side (right panel). Middle: 60x magnification in the highlighted area from 4x image (green, TH; red, Kv4.3). Bottom, left: zoom-in on an example ROI (highlighted in 60x image). Bottom, right: color-coded Kv4.3-channel immunohistochemical signal intensity in the example ROI. (G) Histogram showing intensity of Kv4.3 immunosignals for all TH-positive ROIs, from ipsilateral, vehicle-infused, side (in orange) and from contralateral side (in green). Inset, same data shown as a cumulative distribution.